Integrated Stress Response Activity Marks Stem Cells in Normal Hematopoiesis and Leukemia

van Galen, Peter; Mbong, Nathan; Kreso, Antonia; Schoof, Erwin M.; Wagenblast, Elvin; Ng, Stanley W.K.; Krivdova, Gabriela; Jin, Liqing; Nakauchi, Hiromitsu; Dick, John E.

Published in:
Cell Reports

DOI:
10.1016/j.celrep.2018.10.021

Publication date:
2018

Document version
Publisher's PDF, also known as Version of record

Report

Cell Reports

Integrated Stress Response Activity Marks Stem Cells in Normal Hematopoiesis and Leukemia

Graphical Abstract

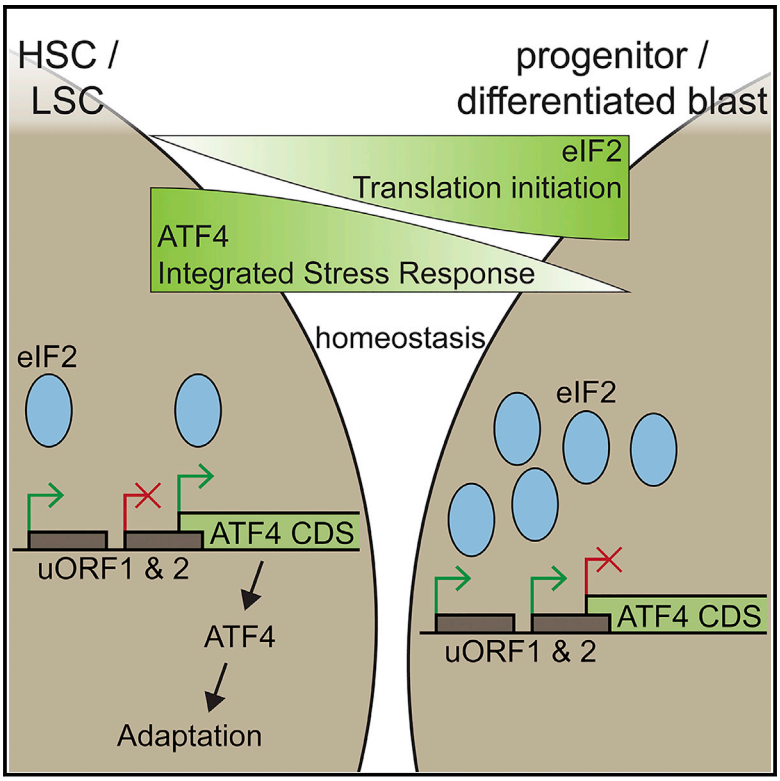

Highlights

- ISR pathway activity in human HSC/MPPs is maintained by low eIF2 and high ATF4
- ATF4 upregulation following amino acid deprivation promotes HSC survival
- Functional HSCs can be purified using an ATF4 reporter that measures ISR activity
- ISR activity marks primitive cells in normal and malignant hematopoietic hierarchies

Authors

Peter van Galen, Nathan Mbong, Antonia Kreso, ..., Liqing Jin, Hiromitsu Nakauchi, John E. Dick

Correspondence

john.dick@uhnresearch.ca

In Brief

Hematopoietic stem cells balance apoptosis with survival to maintain lifelong integrity of the blood system. Van Galen et al. show that specific translation dynamics prime normal and leukemia stem cells to activate the integrated stress response, which can enhance survival in the presence of stressors such as amino acid deprivation.

van Galen et al., 2018, Cell Reports *25*, 1109–1117
October 30, 2018
https://doi.org/10.1016/j.celrep.2018.10.021

CellPress

Cell Reports
Report

Integrated Stress Response Activity Marks Stem Cells in Normal Hematopoiesis and Leukemia

Peter van Galen,[1,9] Nathan Mbong,[2,9] Antonia Kreso,[3] Erwin M. Schoof,[4] Elvin Wagenblast,[2] Stanley W.K. Ng,[2,5] Gabriela Krivdova,[2,6] Liqing Jin,[2] Hiromitsu Nakauchi,[7,8] and John E. Dick[2,6,10,*]

[1]Department of Pathology, Massachusetts General Hospital, Boston, MA 02114, USA
[2]Princess Margaret Cancer Centre, University Health Network, Toronto, ON M5G 1L7, Canada
[3]Department of Surgery, Massachusetts General Hospital, Boston, MA 02114, USA
[4]The Finsen Laboratory, Rigshospitalet/Biotech Research and Innovation Centre (BRIC), Faculty of Health Sciences, University of Copenhagen, 2200 Copenhagen, Denmark
[5]Institute of Biomaterials and Biomedical Engineering, University of Toronto, Toronto, ON M5G 1A1, Canada
[6]Department of Molecular Genetics, University of Toronto, Toronto, ON M5S 1A8, Canada
[7]Division of Stem Cell Therapy, Center for Stem Cell Biology and Regenerative Medicine, Institute of Medical Science, University of Tokyo, Tokyo 108-8639, Japan
[8]Institute for Stem Cell Biology and Regenerative Medicine, Stanford University School of Medicine, Stanford, CA 94305, USA
[9]These authors contributed equally
[10]Lead Contact
*Correspondence: john.dick@uhnresearch.ca
https://doi.org/10.1016/j.celrep.2018.10.021

SUMMARY

Lifelong maintenance of the blood system requires equilibrium between clearance of damaged hematopoietic stem cells (HSCs) and long-term survival of the HSC pool. Severe perturbations of cellular homeostasis result in rapid HSC loss to maintain clonal purity. However, normal homeostatic processes can also generate lower-level stress; how HSCs survive these conditions remains unknown. Here we show that the integrated stress response (ISR) is uniquely active in HSCs and facilitates their persistence. Activating transcription factor 4 (ATF4) mediates the ISR and is highly expressed in HSCs due to scarcity of the eIF2 translation initiation complex. Amino acid deprivation results in eIF2α phosphorylation-dependent upregulation of ATF4, promoting HSC survival. Primitive acute myeloid leukemia (AML) cells also display eIF2 scarcity and ISR activity marks leukemia stem cells (LSCs) in primary AML samples. These findings identify a link between the ISR and stem cell survival in the normal and leukemic contexts.

INTRODUCTION

Replenishment of the blood system throughout the lifetime of an organism requires longevity and integrity of the stem cell pool. However, human HSCs are sensitive to perturbations of cellular homeostasis and prone to undergo apoptosis. The induction of reactive oxygen species (ROS) and accumulation of DNA damage leads to heightened apoptosis of HSCs compared to downstream progenitor cells (Milyavsky et al., 2010; Yahata et al., 2011). Likewise, endoplasmic reticulum (ER) stress causes strong activation of the unfolded protein response in HSCs, resulting in increased apoptosis compared to progenitor cells (Miharada et al., 2014; van Galen et al., 2014a). These responses promote stem cell pool integrity by purging damaged stem cells, but to ensure longevity, HSCs also must be able to survive perturbations that regularly occur during homeostasis such as DNA damage and calorie restriction (Ho et al., 2017; Warr et al., 2013). The signals that ensure persistence of HSCs in the context of lower-level stress caused by metabolic processes during normal homeostasis are unknown.

Many stressors converge on the ISR pathway. This pathway serves to balance stress signals that activate cell death pathways with those that protect the cell to enable restoration of cellular homeostasis (Pakos-Zebrucka et al., 2016). In low-stress conditions, the ISR favors survival as a consequence of the intrinsic stability of adaptive mRNAs and proteins, whereas high stress levels tip the balance toward distal ISR targets that promote cell death (Han et al., 2013; Rutkowski et al., 2006). This survival-death equilibrium is maintained by four stress-inducible kinases: GCN2, PKR, HRI, and PERK (Figure 1A). These kinases phosphorylate eIF2α, a subunit of the eIF2 complex (consisting of eIF2α, β, and γ), thereby preventing formation of the ternary complex (eIF2, GTP, and Met-tRNA$_i$) (Aitken and Lorsch, 2012). This leads to attenuation of global translation initiation, which conserves amino acid pools for essential cellular functions, relieves chaperones of their load, and lowers metabolic demands associated with protein synthesis (Wek et al., 2006). Thus, the ISR integrates many different stressors and initiates global translational attenuation as a protective mechanism.

Highly regulated translation dynamics are critical for HSCs, and recent studies revealed the importance of ribosomal proteins and translation factors to maintain stem cell self-renewal and lineage commitment (Blanco et al., 2016; Cai et al., 2015; Khajuria et al., 2018; Signer et al., 2014, 2016). The ISR delays translation initiation through eIF2α phosphorylation. Paradoxically, ISR-induced eIF2α phosphorylation increases translation of specific transcription factors including activating transcription factor 4 (ATF4), ATF5, and CHOP (*DDIT3*), with ATF4 being the

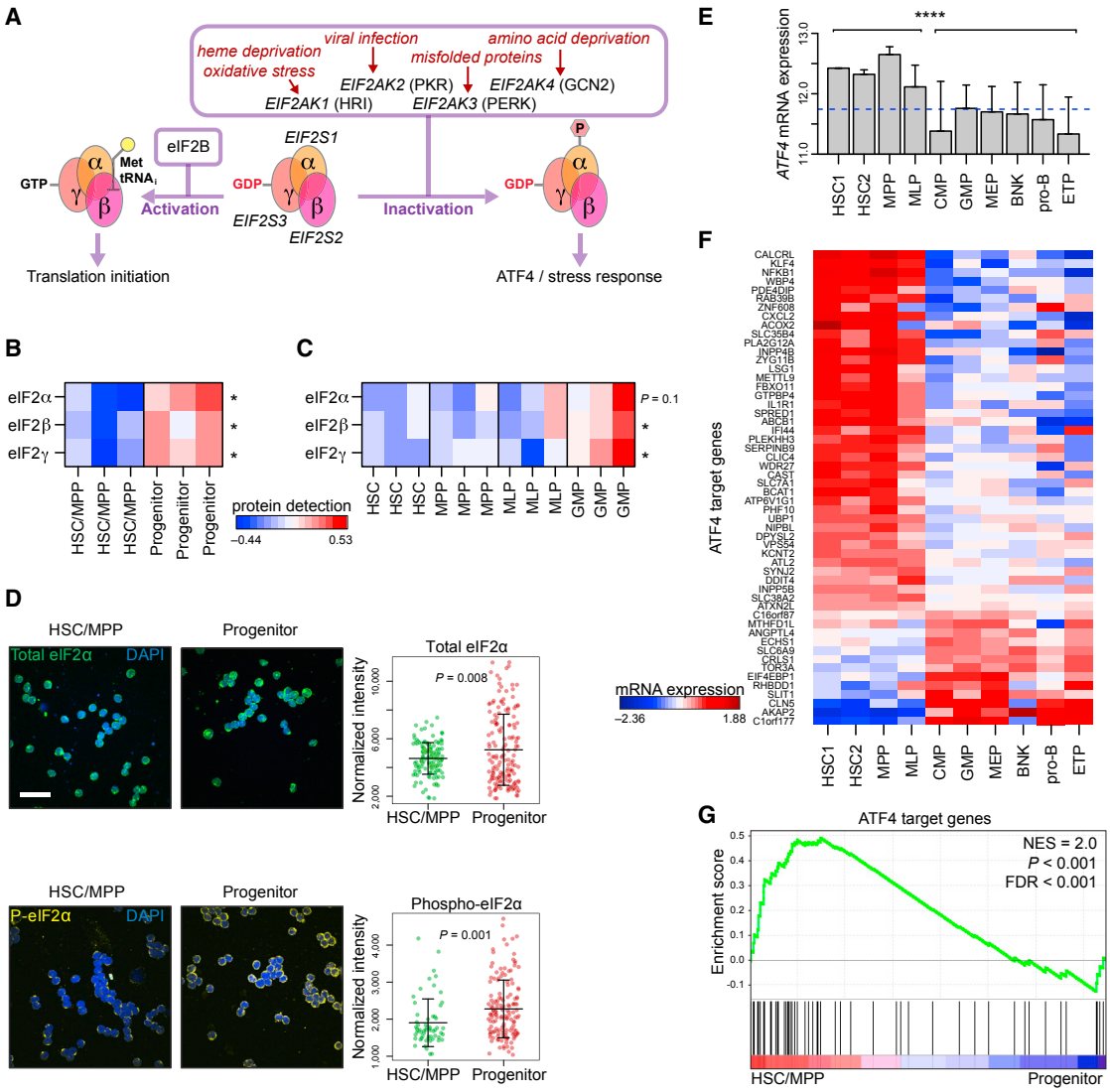

Figure 1. High Integrated Stress Response Activity in HSC/MPPs Compared to Progenitors

(A) Graphic depicts activation of eIF2 translation initiation complex (consisting of α-, β-, and γ-subunits) by GDP/GTP exchange, resulting in assembly of the ternary complex (eIF2, GTP, and Met-tRNA$_i$). In contrast, activation of stress-responsive eIF2α kinases leads to global translational attenuation and upregulation of ATF4 and downstream stress response factors.

(B and C) Heatmaps show protein detection by label-free mass spectrometry in (B) HSC/MPP and progenitor cells or (C) highly purified Lin$^-$ CB populations. Data for n = 3 biological replicates are shown. Colors indicate normalized protein quantities (log$_2$ and centered). The p values indicate comparison between (B) HSC/MPP and progenitor cells or between (C) HSC and GMP.

(D) Immunohistochemistry images and analysis show detection of total eIF2α in HSC/MPP (n = 139) and progenitor (n = 163) cells, and P-eIF2α in HSC/MPP (n = 59) and progenitor (n = 151) cells. Scale bar, 40 μm. Error bars indicate mean ± SD.

(E) Bar graph indicates *ATF4* mRNA expression in sorted CB populations. Dashed blue line indicates the 80th percentile of 29,331 microarray probes (Laurenti et al., 2013). Log$_2$ values of three *ATF4* mRNA probes are shown as mean ± SD, equalized for HSC1 detection. The p value indicates higher *ATF4* expression in primitive cells.

(F) Heatmap shows expression of ATF4 target genes that are differentially expressed between HSC/MPP (HSC1, HSC2, MPP) and myeloid progenitor cells (CMP, GMP, MEP, p < 0.01; see STAR Methods). Microarray values are log$_2$ transformed and centered (Laurenti et al., 2013).

(G) Gene set enrichment analysis shows ATF4 targets from (F) in a gene list ranked by the fold difference between HSC/MPP and myeloid progenitor cells.

*p < 0.05, ****p < 0.0001. See also Table S1 and Figure S1.

most direct ISR effector (Pakos-Zebrucka et al., 2016). Mechanistically, ternary complex scarcity leads to ribosomal bypass of an inhibitory upstream open reading frame (uORF) in the *ATF4* mRNA, leading to efficient ATF4 translation and protein upregulation (Lu et al., 2004). Transcriptional targets of ATF4 include regulators of amino acid metabolism, redox balance,

autophagy, and protein synthesis (B'chir et al., 2013; Han et al., 2013; Harding et al., 2003). Thus, ISR activation results in efficient translation of ATF4, which in turn activates gene networks to facilitate restoration of cellular homeostasis.

The ISR regulates cellular homeostasis in various tissues and cancer cells, but it has typically been studied in bulk populations. Whether the ISR plays distinct roles within the individual cells that make up a tissue hierarchy like the hematopoietic system is unknown. By monitoring ATF4 activity in normal and malignant blood cells, we show that the pro-survival ISR pathway is integral to modulating stem cell stress responses.

RESULTS

High Integrated Stress Response Activity in HSC/MPPs Compared to Progenitors

To assess the expression levels of key ISR pathway components, we analyzed the proteome of purified human HSCs and progenitor cells. Quantitative label-free mass spectrometry revealed lower protein levels of eIF2α, eIF2β, and eIF2γ in HSC/MPPs (multipotent progenitors) compared to downstream progenitors (Figure 1B; Table S1) (E.M.S., S. Xie, A. Mitchell, K.B. Kaufmann, Y. Ge, E. Lechman, T. Kislinger, B.T. Porse, J.E.D., unpublished data). Analysis of more highly purified HSC and progenitor populations showed that eIF2 subunits are similarly expressed in HSCs, MPPs, and multilymphoid progenitors (MLPs), but upregulated in downstream granulocyte-macrophage progenitors (GMPs) (Figure 1C), which is also seen in mouse hematopoiesis (Klimmeck et al., 2012; Signer et al., 2014). To assess levels of total and phosphorylated eIF2α (P-eIF2α), we used immunohistochemistry and intracellular flow cytometry. Within the progenitor compartment, we observed heterogeneity with low and high expression of eIF2α, which may represent different levels within committed progenitor cells of the erythroid, myeloid, and lymphoid lineages. In HSC/MPPs, levels of eIF2α and P-eIF2α were lower on average than in progenitors (Figure 1D; Figures S1A–S1C). The eIF2α kinase PKR was lower in HSC/MPPs compared to progenitors, whereas GCN2 showed an opposite trend (Figure S1D). These data show that key ISR components are distinctly regulated within the hematopoietic hierarchy and that eIF2α, β, and γ protein levels are low in HSC/MPPs.

Low eIF2-GTP-Met-tRNA$_i$ ternary complex leads to efficient translation of ATF4, the principal transcription factor that activates ISR target genes. To gain more insight into ATF4 regulation and activity in HSCs and progenitor cells, we used gene expression data from sorted stem and progenitor cell populations from lineage-depleted cord blood (lin$^-$ CB) (Laurenti et al., 2013). *ATF4* mRNA is highly expressed in CB progenitor cells (mean detection of three *ATF4* probes is in the top 20% of 29,331 probes). Furthermore, *ATF4* expression is higher in HSC/MPPs compared to progenitors, consistent with previous qPCR results (van Galen et al., 2014a) (Figure 1E). Of the 225 recently identified ATF4 target genes (Han et al., 2013), 54 were differentially expressed between HSC/MPP and myeloid progenitor cells (Figure 1F; STAR Methods). Gene set enrichment analysis showed that this set of 54 ATF4 target genes is significantly enriched in HSC/MPPs compared to progenitor cells (false discovery rate [FDR] < 0.001; Figure 1G), suggesting that ATF4 is active in HSCs and contributes to the transcriptional activation of ISR target genes.

ATF4 Reporter Measures ISR Activation

To monitor ATF4 translation, we utilized a lentiviral ATF4 reporter (ATF4^{rep}) that increases translation of an ATF4-GFP fusion gene under conditions of stress that result in eIF2α phosphorylation (Figure S2A) (van Galen et al., 2014a). To determine the specificity of the ATF4^{rep} to different kinds of stress, we transduced TLS-ERG-immortalized cord blood cells (TEX cells) with the ATF4^{rep} and treated them with various stressors. As expected, the ER stress agent thapsigargin, which is commonly used to induce eIF2α phosphorylation, increased ATF4^{rep} 2.1-fold, as measured by the transgene ratio (TGR) between GFP and TagBFP (Figure 2A; STAR Methods). In contrast, bortezomib, which disrupts proteostasis but is not known to function through the ISR, did not cause a notable increase of the ATF4^{rep} TGR. Similarly, the mTOR inhibitor temsirolimus, the translation elongation inhibitor cycloheximide, and the histone deacetylase inhibitor valproic acid did not induce ATF4^{rep}, despite having an impact on cell viability (Figure S2B). Negative and positive control vectors showed no change of the ATF4^{rep} TGR (Figures S2C and S2D). Collectively, these results indicate that the ATF4^{rep} is efficiently induced by ISR activation but not by stressors that are independent of the ISR.

To assess the functionality of the ATF4^{rep} in primary human blood stem and progenitor cells, we transduced lin$^-$ CB cells with the ATF4^{rep} and assessed ATF4 protein levels in sorted GFP-high and GFP-low cells (Figure 2B). ATF4 protein levels were higher in GFP-high cells, indicating that GFP provides a measure for the level of endogenous ATF4. We previously showed that severe tunicamycin-induced ER stress activates the ATF4^{rep} in lin$^-$ CB cells (van Galen et al., 2014a). Other conditions, such as oxidative stress or amino acid deprivation, may lead to less severe stress in the native environment of HSCs. We subjected ATF4^{rep}-transduced CD34$^+$ CB cells to hypoxia and valine depletion, the latter of which strongly induced ATF4^{rep} activation (Figure 2C). More broadly, depletion of 13 amino acids induced the ATF4^{rep} in lin$^-$ CB cells (Figure 2D). Thus, amino acid deprivation strongly induces ISR activation and ATF4 translation in primitive human CB cells.

ATF4 Upregulation through eIF2α Phosphorylation Promotes CB Cell Survival

Phosphorylation of eIF2α reduces ternary complex availability and increases ATF4 levels because slow translation reinitiation favors the ATF4 ORF instead of the inhibitory uORF2 (Figure S2A) (Lu et al., 2004). To investigate whether ATF4^{rep} activation following valine depletion depends on eIF2α phosphorylation, we transduced CD34$^+$ CB cells with overexpression vectors of wild-type eIF2α and eIF2α^{S52A}, a mutant protein that cannot be inactivated by phosphorylation. Following overexpression of wild-type eIF2α, valine depletion resulted in strong ATF4^{rep} activation in CD34$^+$ CB cells (10-fold TGR increase; Figure 2E). In contrast, overexpression of eIF2α^{S52A} abolished valine depletion-induced activation of the ATF4^{rep}, indicating that eIF2α phosphorylation is responsible for ATF4 upregulation following

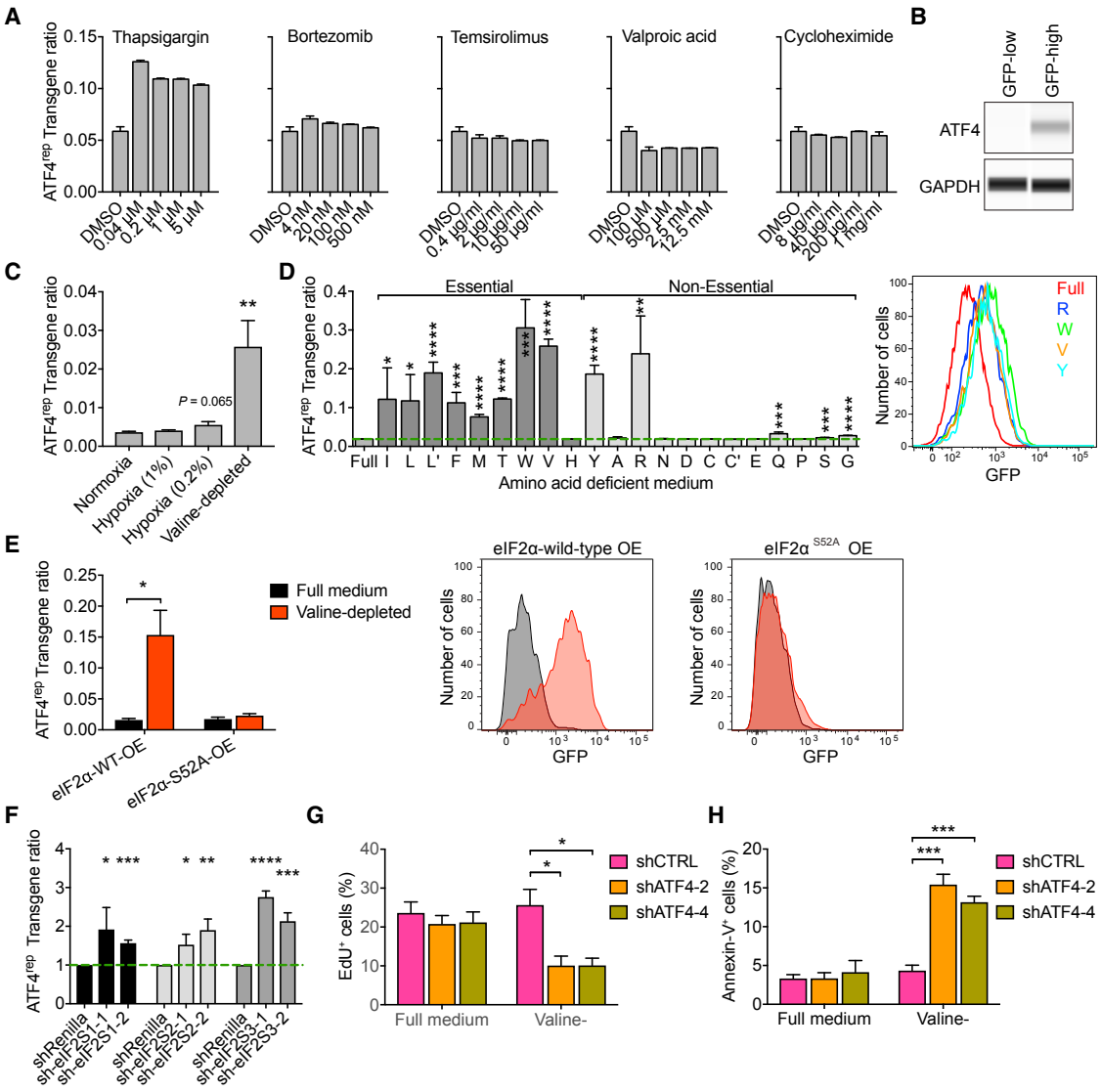

Figure 2. ISR Activates the ATF4 Reporter and Protects against Valine Depletion

(A) Bar plots show TGR of ATF4^{rep}-transduced TEX cells that were treated with indicated stressors. Data are shown as mean ± SD of n = 2 technical replicates, representative of n = 3 similar experiments.

(B) Western blot shows ATF4 levels in sorted GFP-low and GFP-high ATF4^{rep}-transduced lin$^-$ CB cells that were treated with thapsigargin. GAPDH is the loading control. Results are representative of n = 2 CB samples.

(C) Bar plots shows ATF4^{rep} TGR of transduced CD34$^+$ CB cells that were cultured in hypoxic conditions or valine deficient media. Data are shown as mean ± SD of n = 2 CB samples.

(D) Bar plot shows ATF4^{rep} TGR of transduced lin$^-$ CB cells that were cultured in complete (full) medium or media depleted of individual amino acids. Data are shown as mean ± SD of n = 3 time points. Flow cytometry histograms show GFP intensity of TagBFP$^+$ cells at indicated conditions. Letters indicate which amino acid is removed; ' indicates hydrochloride.

(E) Bar plot shows TGR of ATF4^{rep}-transduced CD34$^+$ CB cells that were co-transduced for overexpression of wild-type eIF2α or eIF2α^{S52A} (marked by mOrange). Data are shown as mean ± SD of n = 3 CB samples. Representative histograms show GFP intensity of mOrange$^+$TagBFP$^+$ CB cells.

(F) Bar plot shows TGR of ATF4^{rep}-transduced CD34$^+$ CB cells that were co-transduced with shRNAs for *eIF2S1*, *eIF2S2*, or *eIF2S3* (marked by mCherry). ATF4^{rep} TGR of mCherry$^+$TagBFP$^+$ cells is shown as mean ± SD for n = 3 CB samples.

(G and H) Bar plots show cell proliferation (G) and apoptosis (H) of CD34$^+$ CB cells that were transduced with shATF4 vectors and cultured without valine. Data are shown as mean ± SD of n = 4 CB samples.

*p < 0.05, **p < 0.01, ***p < 0.001, ****p < 0.0001. See also Figure S2.

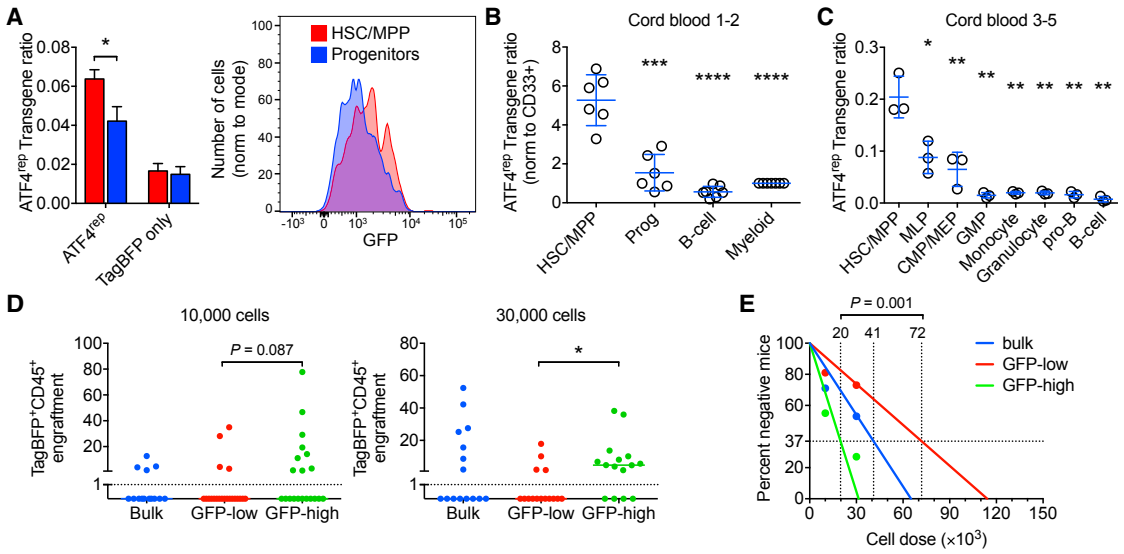

Figure 3. Human HSC/MPPs Display High ISR Activity under Basal Conditions

(A) Bar plot shows ATF4^{rep} TGR of CB cells, 4 days after sorting and transduction. TagBFP-only cells were transduced with a vector lacking the ATF4-GFP transgene. Data are shown as mean ± SEM of n = 4 CB samples. Representative histogram shows GFP intensity of TagBFP$^+$ cells.

(B and C) Scatter column plots show ATF4^{rep} TGR in CB cell populations, isolated from engrafted mice. (B) Each symbol represents the BM of one mouse. Data from n = 2 CB samples are normalized to CD33+ cells. (C) Each symbol represents one BM pool, combined from several mice, for n = 3 CB samples. The p values indicate comparisons to HSC/MPP fractions. Error bars indicate mean ± SD.

(D) Scatter column plots show engraftment of lin$^-$ CB cells that were transduced, sorted based on ATF4^{rep} TGR, and injected into mice. Every symbol represents CD45$^+$TagBFP$^+$ engraftment in one mouse; line is at median (zero in most cases). Pooled data from n = 4 CB samples are shown.

(E) Limiting dilution analysis shows the frequency of engrafting cells in bulk, GFP-low, and GFP-high lin$^-$ CB cell populations. Pooled data from n = 4 CB samples are shown (same as in D).

*p < 0.05, **p < 0.01, ***p < 0.001, ****p < 0.0001. See also Figure S3.

valine depletion. Knockdown of eIF2α, eIF2β, or eIF2γ increased ATF4^{rep} activity (Figure S2E; Figure 2F), indicating that eIF2 availability regulates ATF4 translation. These data establish that valine depletion leads to eIF2α phosphorylation, which reduces ternary complex availability resulting in efficient ATF4 translation.

ATF4 upregulation can induce an adaptive response to diverse stimuli such as oxidative stress, whereas the same pathway can induce apoptosis following severe or prolonged stress (Pakos-Zebrucka et al., 2016). To assess the effect of ATF4 upregulation on survival of CB cells undergoing valine deprivation, we used short hairpin RNA (shRNA) to knock down *ATF4* transcript levels (Figure S2F). Following knockdown of *ATF4* in CD34$^+$ CB cells, the cells were incubated in valine deficient media to induce translational upregulation of ATF4. Valine depletion of non-targeting short hairpin RNA (shCTRL)-transduced cells for 2 days did not affect proliferation or apoptosis, as measured by EdU incorporation and Annexin-V (Figures 2G and 2H). In contrast, valine depletion of shATF4-transduced cells resulted in decreased proliferation (2-fold, p = 0.0004; Figure 2G) and increased apoptosis (4-fold, p < 0.0001; Figure 2H). Thus, ATF4 promotes cell survival of primitive CD34$^+$ CB cells undergoing valine depletion.

Human HSC/MPPs Display High ISR Activity under Basal Conditions

To assess ISR activity across the human hematopoietic hierarchy, we sorted CD34$^+$CD38$^-$ HSC/MPPs and CD34$^+$CD38$^+$ progenitors from lin$^-$ CB and transduced them with the ATF4^{rep}. After 4 days in culture, ATF4^{rep} TGR was 1.6-fold higher in HSC/MPPs compared to progenitors (Figure 3A; Figure S3A), indicating that HSC/MPPs have high ISR activity compared to committed progenitors *in vitro*. Since *in vitro* culture could induce stress, we sought to undertake *in vivo* xenograft studies to examine HSC/MPP and progenitors in the best available setting to approximate homeostatic conditions for human cells. Transplantation of ATF4^{rep}-transduced lin$^-$ CB cells showed that human HSC/MPPs in the mouse bone marrow (BM) maintained a 2.4-fold higher ATF4^{rep} TGR compared to downstream progenitors (Figure 3B). Furthermore, HSC/MPPs displayed a 2.3-fold higher ATF4^{rep} TGR in comparison to closely related MLPs (Figure 3C). ATF4^{rep} TGR further declined in downstream common myeloid progenitor and megakaryocyte-erythroid progenitor (CMP and MEP) populations and, compared to HSC/MPPs, was 13-fold lower within mature monocytes, granulocytes, pro-B, and B cells (Figure 3C). These results indicate that HSCs display higher ISR activity than progenitors when assessed in basal conditions, which may contribute to HSC endurance.

To determine if the high ISR activity in HSCs is associated with improved survival, we transplanted lin$^-$ CB cells expressing high ATF4^{rep} activity (GFP-high) and low ATF4^{rep} activity (GFP-low) into mice (Figure S3B). The level of engraftment from GFP-high cells was increased compared to GFP-low cells (Figure 3D). Furthermore, the number of engrafted mice from GFP-high cells

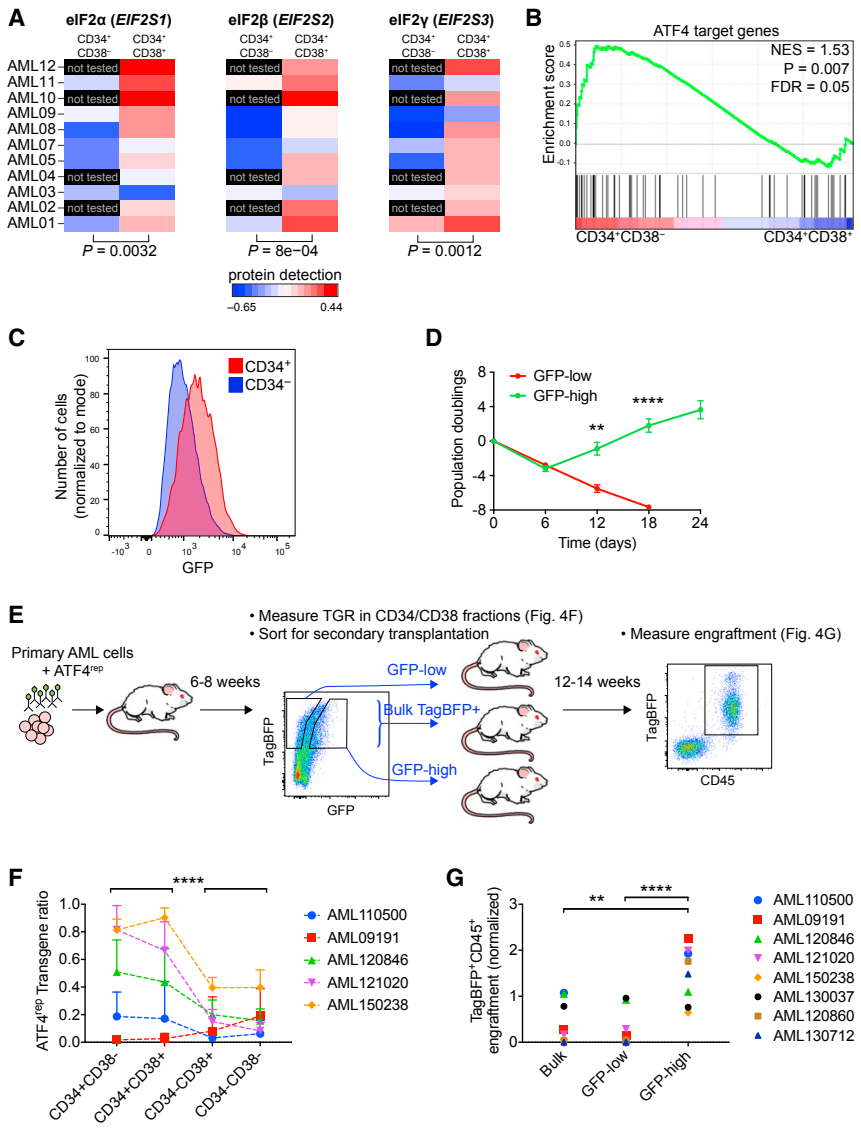

Figure 4. Enrichment of Human LSCs Based on High ISR Levels

(A) Heatmaps show protein detection by label-free mass spectrometry in sorted $CD34^+CD38^-$ and $CD34^+CD38^+$ cells from 11 AML patients. Some fractions are not tested because we could not obtain a sufficient number of cells to perform mass spectrometry. Colors indicate normalized protein quantities (log_2 and centered).

(B) Gene set enrichment analysis shows ATF4 targets (from Figure 1F) in a gene list ranked by the fold difference between sorted $CD34^+CD38^-$ and $CD34^+CD38^+$ AML cells. mRNA expression in AML fractions was previously assessed by RNA sequencing (RNA-seq) (Ng et al., 2016).

(C) Flow histogram shows GFP intensity of primitive ($CD34^+$) and differentiated ($CD34^-$) $ATF4^{rep}$-transduced $TagBFP^+$ 8227 cells. Results are representative of n = 2 independent experiments.

(D) Line graph shows population doublings of sorted 8227 cells. Viable cells were counted at 6-day intervals. Data are shown as mean ± SD of n = 3 technical replicates.

(E) Graphic overview of experiment to assess $ATF4^{rep}$ TGR in AML CD34/CD38 populations, and secondary transplantation to assess LSC potential of GFP-low and GFP-high AML cells.

(F) Line graph shows $ATF4^{rep}$ TGR in phenotypic fractions of human AML samples that were isolated from engrafted mice. Each symbol represents mean ± SD of ≥ 5 mice; results were normalized to the maximum TGR of that experiment.

(G) Dot plots show secondary engraftment levels of AML cells that were recovered from primary mice, sorted based on $ATF4^{rep}$ TGR, and re-transplanted. Every dot represents median secondary engraftment (normalized to the average) of one AML sample.

*p < 0.05, ****p < 0.0001. See also Figures S3 and S4.

was increased compared to GFP-low cells. Using limiting dilution analysis, we calculated that the frequency of engrafting cells was 1 in 19,804 cells in the GFP-high population and 1 in 71,922 cells in the GFP-low population; bulk $TagBFP^+$ cells possessed an intermediate HSC frequency of 1 in 41,046 cells (Figure 3E; Figure S3C). Thus, cells that efficiently translate ATF4 are robust and survive transplantation, indicating that high ISR activity marks functional HSCs.

Enrichment of Human LSCs Based on High ISR Levels

The hierarchical structure of normal hematopoiesis is partially maintained in acute myeloid leukemia (AML) and leukemia stem cells (LSCs) that share numerous stemness properties with normal HSCs are responsible for disease propagation (Dick, 2008). We examined the expression of central ISR components in AML cell populations. Similar to our findings in normal CB cells, mass spectrometry revealed lower protein levels of eIF2α, eIF2β, and eIF2γ in phenotypically primitive ($CD34^+$ $CD38^-$) compared to differentiated ($CD34^+CD38^+$) AML cell populations (Figure 4A). Gene set enrichment analysis of 54 ATF4 target genes showed enrichment in primitive AML cells (Figure 4B). Similar trends were observed when we compared functionally validated LSC^+ versus LSC^- populations for eIF2β and eIF2γ protein detection (Figure S3D) and ATF4 target mRNA expression (Figure S3E). Low eIF2 levels and high ATF4 target gene expression suggest that the high ISR activity we observed in normal HSC/MPPs is conserved in LSCs.

To determine if ISR activity could be used to separate functionally distinct AML cell populations, we examined $ATF4^{rep}$ expression in human AML cells. Using the 8227 AML cell culture system, which maintains hierarchical organization *in vitro* (Lechman et al., 2016), we found that primitive $CD34^+CD38^-$ cells displayed the highest $ATF4^{rep}$ TGR, which progressively declined in downstream progenitors (Figure 4C; Figure S3F). We sorted GFP-high and GFP-low populations from $ATF4^{rep}$-transduced

8227 AML cells and assessed culture-initiating capacity, a surrogate assay for LSC function. Only GFP-high cells were able to expand in culture for over 3 weeks (Figure 4D), indicating that ATF4^{rep} activity can be used to prospectively isolate cells that display features of primitive LSCs.

We wanted to evaluate ATF4^{rep} expression in the malignant hierarchy using primary AML patient samples. Since *in vitro* expansion of primary AML cells is challenging and does not maintain the developmental hierarchy, we transduced AML cells with the ATF4^{rep} and established AML in immunodeficient mice (Figure 4E; Table S2). After 6–8 weeks, mice were sacrificed and human AML cells were assessed for CD34/CD38 expression and ATF4^{rep} TGR by flow cytometry. In four out of five samples, the ATF4^{rep} TGR was higher in CD34^{+} compared to CD34^{-} cells (Figure 4F; Figure S4A). AML09191 was an exception, showing higher ATF4^{rep} TGR in CD34^{-} compared to CD34^{+} cells. Taken together, these ATF4^{rep} measurements suggest that most primary AML samples have high ISR activity in phenotypically primitive cells.

Although CD34 can enrich for LSCs in most AML cases, the surface phenotype of AML cells can be decoupled from LSC activity. To test whether primary AML cells that possess high ISR activity are enriched for LSC function, we sorted TagBFP^{+} (bulk), GFP-low and GFP-high populations and transplanted cells into secondary recipient mice (Figure 4E). GFP-high cells showed higher engraftment in three out of eight samples, with two additional samples showing the same trend (Figure S4B). In AML09191, GFP-high cells showed higher engraftment, indicating that ATF4^{rep} activity maintained its correlation with LSC activity despite its negative correlation with CD34 expression. On average, GFP-high cells showed 8.5-fold higher secondary engraftment than GFP-low cells ($p < 0.0001$; Figure 4G). These data indicate that high ISR activity is associated with normal and malignant stem cells.

DISCUSSION

Our data establish that the ISR-mediated pro-survival program is uniquely wired in HSCs where it plays a role in governing HSC function. The tendency of HSCs to undergo apoptosis following stress and damage (Milyavsky et al., 2010; van Galen et al., 2014a; Yahata et al., 2011) needs to be balanced with alleviation of low-level perturbations that occur under homeostasis to ensure HSC functionality. Our results show that amino acid deprivation is one such perturbation where ATF4-dependent pro-survival signals play a protective role. We show that high expression of the ISR effector ATF4 is contingent on eIF2 scarcity, representing a mechanism of ISR activity that may also safeguard stem cells in other tissues (Blanco et al., 2016; Zismanov et al., 2016). ATF4 is modulated by additional signals including mTOR and post-translational modifications (Ben-Sahra et al., 2016; Wortel et al., 2017). Several processes that are important for HSC maintenance are regulated by ATF4, including autophagy, amino acid metabolism and oxidative stress resistance (B'chir et al., 2013; Harding et al., 2003; Ho et al., 2017; Taya et al., 2016). Accordingly, ATF4-mediated reduction of oxidative stress has been implicated to maintain erythropoiesis and HSC development in mice (Suragani et al., 2012; Zhao et al., 2015). Additional studies are required to elucidate the full complement of signals upstream and downstream of ATF4 in different conditions. In cancer, ATF4 has been shown to confer resistance to nutrient deprivation, hypoxia, and ROS (Rouschop et al., 2013; Ye et al., 2010). Considering the protective role of ATF4 for HSCs undergoing valine depletion, AML therapies that affect amino acid metabolism should take into account ATF4-dependent adaptive mechanisms (Heydt et al., 2018; Jacque et al., 2015; Miraki-Moud et al., 2015; Willems et al., 2013). The conservation of ISR signaling in primitive CB and a subset of primary AML samples supports the possibility of targeting LSCs through the ISR pathway and underscores the importance of monitoring adaptive responses in developmentally distinct cancer cell subpopulations. Further evaluation of eIF2α phosphorylation and its upstream kinases in activation of the ISR and how this is differentially regulated in HSC and specific progenitor subsets may inform strategies to modulate this pathway and stem cell fate outcomes. Understanding the interplay between stemness, translational control, and stress signaling is needed to manipulate stem cells for therapeutic purposes, such as promoting HSC survival during transplantation and gene therapy or targeting the survival of LSCs.

STAR★METHODS

Detailed methods are provided in the online version of this paper and include the following:

- KEY RESOURCES TABLE
- CONTACT FOR REAGENT AND RESOURCE SHARING
- EXPERIMENTAL MODEL AND SUBJECT DETAILS
  - Cord blood (CB) and acute myeloid leukemia (AML) samples
  - CB, TEX, and 8227 cell preparation and liquid culture
  - Mouse xenotransplantation
- METHOD DETAILS
  - Lentiviral vectors
  - shRNA knock-down constructs
  - Quantitative PCR
  - Amino acid depletion
  - Thapsigargin, cycloheximide, valproic acid, temsirolimus, and bortezomib
  - Mass spectrometry
  - Fluorescence-Activated Cell Sorting (FACS) and intracellular flow cytometry
  - Apoptosis and cell proliferation assays
  - Immunofluorescence
  - Western blot
  - Transcriptional analysis
- QUANTIFICATION AND STATISTICAL ANALYSIS
- DATA AND SOFTWARE AVAILABILITY

SUPPLEMENTAL INFORMATION

Supplemental Information includes four figures and three tables can be found with this article online at https://doi.org/10.1016/j.celrep.2018.10.021.

ACKNOWLEDGMENTS

We thank David Ron, Brad Wouters, Adam Wilkinson, Elisa Laurenti, and all Dick lab members for critical advice; the obstetrics units of Trillium Health Partners (Mississauga and Credit Valley sites) for CB units; and the SickKids-UHN flow facility staff for technical support. P.v.G. is a Leukemia and Lymphoma Society Fellow (5458-17). E.M.S. is supported by the European Molecular Biology Organization (ALTF 1595-2014), the European Commission (LTFCOFUND2013, GA-2013-609409), and Marie Curie Actions. E.W. is supported by the Human Frontier Science Program. The work in J.E.D.'s lab is funded by the Canadian Institutes for Health Research, Canadian Cancer Society Research Institute, Terry Fox Foundation, Genome Canada through the Ontario Genomics Institute, Ontario Institute for Cancer Research, a Canada Research Chair, the Princess Margaret Hospital Foundation, and the Ontario Ministry of Health and Long Term Care (OMOHLTC). The views expressed in this manuscript do not necessarily reflect those of the OMOHLTC.

AUTHOR CONTRIBUTIONS

P.v.G., N.M., A.K., and J.E.D. conceptualized the study. P.v.G., N.M., A.K., E.M.S., E.W., S.W.K.N., G.K., and L.J. performed experiments and analyzed the data. P.v.G., E.M.S., and S.W.K.N. performed bioinformatic analyses. H.N. provided reagents and expertise. P.v.G. and N.M. wrote the paper. A.K. and J.E.D. revised the paper. J.E.D. supervised the study.

DECLARATION OF INTERESTS

J.E.D. has sponsored research agreements with Celgene and is on the Scientific Advisory Board of Trillium Therapeutics.

Received: April 5, 2018
Revised: July 25, 2018
Accepted: October 2, 2018
Published: October 30, 2018

REFERENCES

Aitken, C.E., and Lorsch, J.R. (2012). A mechanistic overview of translation initiation in eukaryotes. Nat. Struct. Mol. Biol. *19*, 568–576.

B'chir, W., Maurin, A.C., Carraro, V., Averous, J., Jousse, C., Muranishi, Y., Parry, L., Stepien, G., Fafournoux, P., and Bruhat, A. (2013). The eIF2α/ATF4 pathway is essential for stress-induced autophagy gene expression. Nucleic Acids Res. *41*, 7683–7699.

Ben-Sahra, I., Hoxhaj, G., Ricoult, S.J.H., Asara, J.M., and Manning, B.D. (2016). mTORC1 induces purine synthesis through control of the mitochondrial tetrahydrofolate cycle. Science *351*, 728–733.

Blanco, S., Bandiera, R., Popis, M., Hussain, S., Lombard, P., Aleksic, J., Sajini, A., Tanna, H., Cortés-Garrido, R., Gkatza, N., et al. (2016). Stem cell function and stress response are controlled by protein synthesis. Nature *534*, 335–340.

Cai, X., Gao, L., Teng, L., Ge, J., Oo, Z.M., Kumar, A.R., Gilliland, D.G., Mason, P.J., Tan, K., and Speck, N.A. (2015). Runx1 deficiency decreases ribosome biogenesis and confers stress resistance to hematopoietic stem and progenitor cells. Cell Stem Cell *17*, 165–177.

Cox, J., and Mann, M. (2008). MaxQuant enables high peptide identification rates, individualized p.p.b.-range mass accuracies and proteome-wide protein quantification. Nat. Biotechnol. *26*, 1367–1372.

Cox, J., Hein, M.Y., Luber, C.A., Paron, I., Nagaraj, N., and Mann, M. (2014). Accurate proteome-wide label-free quantification by delayed normalization and maximal peptide ratio extraction, termed MaxLFQ. Mol. Cell. Proteomics *13*, 2513–2526.

Dick, J.E. (2008). Stem cell concepts renew cancer research. Blood *112*, 4793–4807.

Han, J., Back, S.H., Hur, J., Lin, Y.H., Gildersleeve, R., Shan, J., Yuan, C.L., Krokowski, D., Wang, S., Hatzoglou, M., et al. (2013). ER-stress-induced transcriptional regulation increases protein synthesis leading to cell death. Nat. Cell Biol. *15*, 481–490.

Harding, H.P., Zhang, Y., Zeng, H., Novoa, I., Lu, P.D., Calfon, M., Sadri, N., Yun, C., Popko, B., Paules, R., et al. (2003). An integrated stress response regulates amino acid metabolism and resistance to oxidative stress. Mol. Cell *11*, 619–633.

Heydt, Q., Larrue, C., Saland, E., Bertoli, S., Sarry, J.E., Besson, A., Manenti, S., Joffre, C., and Mansat-De Mas, V. (2018). Oncogenic FLT3-ITD supports autophagy via ATF4 in acute myeloid leukemia. Oncogene *37*, 787–797.

Ho, T.T., Warr, M.R., Adelman, E.R., Lansinger, O.M., Flach, J., Verovskaya, E.V., Figueroa, M.E., and Passegué, E. (2017). Autophagy maintains the metabolism and function of young and old stem cells. Nature *543*, 205–210.

Hu, Y., and Smyth, G.K. (2009). ELDA: extreme limiting dilution analysis for comparing depleted and enriched populations in stem cell and other assays. J. Immunol. Methods *347*, 70–78.

Jacque, N., Ronchetti, A.M., Larrue, C., Meunier, G., Birsen, R., Willems, L., Saland, E., Decroocq, J., Maciel, T.T., Lambert, M., et al. (2015). Targeting glutaminolysis has antileukemic activity in acute myeloid leukemia and synergizes with BCL-2 inhibition. Blood *126*, 1346–1356.

Khajuria, R.K., Munschauer, M., Ulirsch, J.C., Fiorini, C., Ludwig, L.S., McFarland, S.K., Abdulhay, N.J., Specht, H., Keshishian, H., Mani, D.R., et al. (2018). Ribosome levels selectively regulate translation and lineage commitment in human hematopoiesis. Cell *173*, 90–103.e19.

Klimmeck, D., Hansson, J., Raffel, S., Vakhrushev, S.Y., Trumpp, A., and Krijgsveld, J. (2012). Proteomic cornerstones of hematopoietic stem cell differentiation: distinct signatures of multipotent progenitors and myeloid committed cells. Mol. Cell. Proteomics *11*, 286–302.

Knott, S.R.V., Maceli, A., Erard, N., Chang, K., Marran, K., Zhou, X., Gordon, A., Demerdash, O.E., Wagenblast, E., Kim, S., et al. (2014). A computational algorithm to predict shRNA potency. Mol. Cell *56*, 796–807.

Laurenti, E., Doulatov, S., Zandi, S., Plumb, I., Chen, J., April, C., Fan, J.B., and Dick, J.E. (2013). The transcriptional architecture of early human hematopoiesis identifies multilevel control of lymphoid commitment. Nat. Immunol. *14*, 756–763.

Lechman, E.R., Gentner, B., Ng, S.W., Schoof, E.M., van Galen, P., Kennedy, J.A., Nucera, S., Ciceri, F., Kaufmann, K.B., Takayama, N., et al. (2016). miR-126 regulates distinct self-renewal outcomes in normal and malignant hematopoietic stem cells. Cancer Cell *29*, 214–228.

Lu, P.D., Harding, H.P., and Ron, D. (2004). Translation reinitiation at alternative open reading frames regulates gene expression in an integrated stress response. J. Cell Biol. *167*, 27–33.

Miharada, K., Sigurdsson, V., and Karlsson, S. (2014). Dppa5 improves hematopoietic stem cell activity by reducing endoplasmic reticulum stress. Cell Rep. *7*, 1381–1392.

Milyavsky, M., Gan, O.I., Trottier, M., Komosa, M., Tabach, O., Notta, F., Lechman, E., Hermans, K.G., Eppert, K., Konovalova, Z., et al. (2010). A distinctive DNA damage response in human hematopoietic stem cells reveals an apoptosis-independent role for p53 in self-renewal. Cell Stem Cell *7*, 186–197.

Miraki-Moud, F., Ghazaly, E., Ariza-McNaughton, L., Hodby, K.A., Clear, A., Anjos-Afonso, F., Liapis, K., Grantham, M., Sohrabi, F., Cavenagh, J., et al. (2015). Arginine deprivation using pegylated arginine deiminase has activity against primary acute myeloid leukemia cells in vivo. Blood *125*, 4060–4068.

Ng, S.W., Mitchell, A., Kennedy, J.A., Chen, W.C., McLeod, J., Ibrahimova, N., Arruda, A., Popescu, A., Gupta, V., Schimmer, A.D., et al. (2016). A 17-gene stemness score for rapid determination of risk in acute leukaemia. Nature *540*, 433–437.

Pakos-Zebrucka, K., Koryga, I., Mnich, K., Ljujic, M., Samali, A., and Gorman, A.M. (2016). The integrated stress response. EMBO Rep. *17*, 1374–1395.

Rouschop, K.M., Dubois, L.J., Keulers, T.G., van den Beucken, T., Lambin, P., Bussink, J., van der Kogel, A.J., Koritzinsky, M., and Wouters, B.G. (2013). PERK/eIF2α signaling protects therapy resistant hypoxic cells through induction of glutathione synthesis and protection against ROS. Proc. Natl. Acad. Sci. USA *110*, 4622–4627.

Rutkowski, D.T., Arnold, S.M., Miller, C.N., Wu, J., Li, J., Gunnison, K.M., Mori, K., Sadighi Akha, A.A., Raden, D., and Kaufman, R.J. (2006). Adaptation to ER stress is mediated by differential stabilities of pro-survival and pro-apoptotic mRNAs and proteins. PLoS Biol. *4*, e374.

Signer, R.A., Magee, J.A., Salic, A., and Morrison, S.J. (2014). Haematopoietic stem cells require a highly regulated protein synthesis rate. Nature *509*, 49–54.

Signer, R.A., Qi, L., Zhao, Z., Thompson, D., Sigova, A.A., Fan, Z.P., DeMartino, G.N., Young, R.A., Sonenberg, N., and Morrison, S.J. (2016). The rate of protein synthesis in hematopoietic stem cells is limited partly by 4E-BPs. Genes Dev. *30*, 1698–1703.

Suragani, R.N., Zachariah, R.S., Velazquez, J.G., Liu, S., Sun, C.W., Townes, T.M., and Chen, J.J. (2012). Heme-regulated eIF2α kinase activated Atf4 signaling pathway in oxidative stress and erythropoiesis. Blood *119*, 5276–5284.

Taya, Y., Ota, Y., Wilkinson, A.C., Kanazawa, A., Watarai, H., Kasai, M., Nakauchi, H., and Yamazaki, S. (2016). Depleting dietary valine permits nonmyeloablative mouse hematopoietic stem cell transplantation. Science *354*, 1152–1155.

van Galen, P., Kreso, A., Mbong, N., Kent, D.G., Fitzmaurice, T., Chambers, J.E., Xie, S., Laurenti, E., Hermans, K., Eppert, K., et al. (2014a). The unfolded protein response governs integrity of the haematopoietic stem-cell pool during stress. Nature *510*, 268–272.

van Galen, P., Kreso, A., Wienholds, E., Laurenti, E., Eppert, K., Lechman, E.R., Mbong, N., Hermans, K., Dobson, S., April, C., et al. (2014b). Reduced lymphoid lineage priming promotes human hematopoietic stem cell expansion. Cell Stem Cell *14*, 94–106.

Warner, J.K., Wang, J.C., Takenaka, K., Doulatov, S., McKenzie, J.L., Harrington, L., and Dick, J.E. (2005). Direct evidence for cooperating genetic events in the leukemic transformation of normal human hematopoietic cells. Leukemia *19*, 1794–1805.

Warr, M.R., Binnewies, M., Flach, J., Reynaud, D., Garg, T., Malhotra, R., Debnath, J., and Passegué, E. (2013). FOXO3A directs a protective autophagy program in haematopoietic stem cells. Nature *494*, 323–327.

Wek, R.C., Jiang, H.Y., and Anthony, T.G. (2006). Coping with stress: eIF2 kinases and translational control. Biochem. Soc. Trans. *34*, 7–11.

Willems, L., Jacque, N., Jacquel, A., Neveux, N., Maciel, T.T., Lambert, M., Schmitt, A., Poulain, L., Green, A.S., Uzunov, M., et al. (2013). Inhibiting glutamine uptake represents an attractive new strategy for treating acute myeloid leukemia. Blood *122*, 3521–3532.

Wortel, I.M.N., van der Meer, L.T., Kilberg, M.S., and van Leeuwen, F.N. (2017). Surviving Stress: Modulation of ATF4-Mediated Stress Responses in Normal and Malignant Cells. Trends Endocrinol. Metab. *28*, 794–806.

Yahata, T., Takanashi, T., Muguruma, Y., Ibrahim, A.A., Matsuzawa, H., Uno, T., Sheng, Y., Onizuka, M., Ito, M., Kato, S., and Ando, K. (2011). Accumulation of oxidative DNA damage restricts the self-renewal capacity of human hematopoietic stem cells. Blood *118*, 2941–2950.

Ye, J., Kumanova, M., Hart, L.S., Sloane, K., Zhang, H., De Panis, D.N., Bobrovnikova-Marjon, E., Diehl, J.A., Ron, D., and Koumenis, C. (2010). The GCN2-ATF4 pathway is critical for tumour cell survival and proliferation in response to nutrient deprivation. EMBO J. *29*, 2082–2096.

Zhao, Y., Zhou, J., Liu, D., Dong, F., Cheng, H., Wang, W., Pang, Y., Wang, Y., Mu, X., Ni, Y., et al. (2015). ATF4 plays a pivotal role in the development of functional hematopoietic stem cells in mouse fetal liver. Blood *126*, 2383–2391.

Zismanov, V., Chichkov, V., Colangelo, V., Jamet, S., Wang, S., Syme, A., Koromilas, A.E., and Crist, C. (2016). Phosphorylation of eIF2α is a translational control mechanism regulating muscle stem cell quiescence and self-renewal. Cell Stem Cell *18*, 79–90.

STAR★METHODS

KEY RESOURCES TABLE

REAGENT or RESOURCE	SOURCE	IDENTIFIER
Antibodies		
Alexa Fluor 488 Goat anti-Rabbit IgG	ThermoFisher Scientific	Cat# A-11034; RRID: AB_2576217
Mouse monoclonal eiF2a (D3)	Santa Cruz Biotech	Cat# sc-133132
Phospho-eIF2a (Ser52)	ThermoFisher Scientific	Cat# 701268; RRID: AB_2532450
Rabbit monoclonal phospho-eIF2a (Ser51)	ThermoFisher Scientific	Cat# 44-728G; RRID: AB_10983400
ATF4-4 (D4B8) Rabbit monoclonal	Cell Signaling	Cat# 11815; RRID: AB_2616025
Rabbit monoclonal GAPDH (14C10)	Cell Signaling	Cat# 2118; RRID: AB_561053
PE-Cy7 Mouse Anti-Human CD38 (HB7)	BD	Cat# 335790
APC-Cy7 Mouse Anti-Human CD34	BD PharMingen	Cat# 624072
APC Mouse Anti-Human CD45 (2D1)	BD	Cat# 340943
PE Mouse Anti-Human CD33 (P67.6)	BD	Cat# 347787
V450 Mouse Anti-Human CD7 (M-T701)	BD	Cat# 642916
PE Mouse Anti-Human CD19 (SJ25C1)	BD	Cat# 340364
PE-Cy5 Mouse Anti-Human CD90	BD PharMingen	Cat# 555597
PE-Cy5 Mouse Anti-Human CD10	Beckman Coulter	Cat# PN IM2721U
Biotin Mouse Anti-Human CD45RA	BD PharMingen	Cat# 555487
PE Mouse Anti-Human CD135 (FLT3)	BD PharMingen	Cat# 558996
PE-Cy5 Mouse Anti-Human CD49f	BD PharMingen	Cat# 551129
Biotin Mouse Anti-Human CD135	BD PharMingen	Cat# 624008
Bacterial and Virus Strains		
Vesicular Stomatitis virus G protein (VSVG)	Addgene	Plasmid# 14888
pMDLg/pRRE plasmid	Addgene	Plasmid# 60488
pRSV-Rev	Addgene	Plasmid# 12253
Biological Samples		
Primary AML Patient Samples	Princess Margaret Cancer Center	
Healthy Human Umbilical Cord Blood Donor	Trillium Health Partners	
Healthy Human Umbilical Cord Blood Donor	Credit Valley Hospital	
Chemicals, Peptides, and Recombinant Proteins		
Stem Cell Factor (SCF)	Miltenyi Biotec	Cat# 130-096-696
Fms-related tyrosine kinase ligand (FLT3-L)	Miltenyi Biotec	Cat# 130-096-474
Human Thrombopoietin (TPO)	Miltenyi Biotec	Cat# 130-095-752
Human Interleukin-6 (IL-6)	Miltenyi Biotec	Cat# 130-093-934
Human Granulocyte-Colony stimulating factor (G-CSF)	Miltenyi Biotec	Cat# 130-094-265
X-Vivo Chemically Defined Serum	Lonza	Cat# 04-380Q
Human Interleukin-3 (IL-3)	Miltenyi Biotec	Cat# 130-095-068
Iscove's Modified Dulbecco's Medium (IMDM)	GIBCO	Cat# 1240053
RIPA Buffer	Thermo Fisher	Cat# 899000
BCA Protein Assay Kit	ThermoFisher Scientific	Cat# 23225
Thapsigargin	Sigma-Aldrich	Cat# T9033
Cycloheximide	Sigma-Aldrich	Cat# C7698
Valproic Acid	Sigma-Aldrich	Cat# PHR1061

(*Continued on next page*)

Continued

REAGENT or RESOURCE	SOURCE	IDENTIFIER
Bortezomib	Cell Signaling	Cat# 2204
Temsirolimus	Sigma-Aldrich	Cat# P20020
Anti-EIF2S1(phospho-S51)	Abcam	Cat# Ab32157; RRID: AB_732117
Critical Commercial Assays		
Click-IT Plus EdU Pacific Blue Flow Cytometry Kit	ThermoFisher Scientific	Cat# 10636
Deposited Data		
CB progenitor microarray	Laurenti et al., 2013	GEO: GSE42414; Processed data, http://jdstemcellresearch.ca/node/32
ATF4 targets	Han et al., 2013	
CB progenitor mass spectrometry	E.M.S., S. Xie, A. Mitchell, K.B. Kaufmann, Y. Ge, E. Lechman, T. Kislinger, B.T. Porse, J.E.D., unpublished data	
AML fractions RNA-seq	Ng et al., 2016	GEO: GSE76009
Experimental Models: Cell Lines		
TEX cells	Dick lab, Princess Margaret Cancer Centre	
8227 cells	Dick lab, Princess Margaret Cancer Centre	
MOLM13	DSMZ	ACC 554
Experimental Models: Organisms/Strains		
NOD/Lt-scid/IL2Rγnull (NSG)	The Jackson Laboratory	005557
Oligonucleotides		
See Table S3 for oligonucleotide sequences.		
Recombinant DNA		
$ATF4^{rep}$	Dick lab, Princess Margaret Cancer Centre	
$ATF4.12^{rep}$	Dick lab, Princess Margaret Cancer Centre	
$ATF4.14^{rep}$	Dick lab, Princess Margaret Cancer Centre	
$eIF2\alpha^{WT}$-OE	Dick lab, Princess Margaret Cancer Centre	
$eIF2\alpha^{S52A}$-OE	Dick lab, Princess Margaret Cancer Centre	
pLBC2	Dick lab, Princess Margaret Cancer Centre	
Software and Algorithms		
FACSDiva	BD	https://www.bdbiosciences.com/us/instruments/research/software/c/2046610
FlowJo10	FlowJo, LLC	https://www.flowjo.com/
Prism 7.0a	GraphPad	https://www.graphpad.com/
Extreme Limiting Dilution Analysis (ELDA)	Hu and Smyth, 2009	http://bioinf.wehi.edu.au/software/elda/
Excel for Mac version 16.17	Microsoft	https://www.microsoft.com/en-us/p/excel-2016-for-mac/cfq7ttc0k5f2
RStudio Version 1.1.456 using R 3.5.1	RStudio	https://www.rstudio.com

CONTACT FOR REAGENT AND RESOURCE SHARING

Further information and requests for resources and reagents should be directed to and will be fulfilled by the Lead Contact, John E. Dick (John.Dick@uhnresearch.ca).

EXPERIMENTAL MODEL AND SUBJECT DETAILS

Cord blood (CB) and acute myeloid leukemia (AML) samples

All human samples were obtained with informed consent according to procedures approved by the Institutional Review Boards of the University Health Network, Trillium Hospital, and/or Credit Valley Hospital. Mononuclear cells were obtained by centrifugation of CB on Ficoll (Ficoll-Paque Premium GE Healthcare) followed by red blood cell lysis with ammonium chloride solution (StemCell

Technologies). Lineage depletion of mononuclear cells was achieved using StemSep Human Progenitor Cell Enrichment Kit according to the manufacturer's protocol (StemCell Technologies). Thawed Lin- CB cells were transduced as described previously (van Galen et al., 2014b). Freshly thawed primary AML samples harvested from patients' peripheral blood were exposed to lentivirus for 19 hours. Details of AML patient samples are outlined in Table S2.

CB, TEX, and 8227 cell preparation and liquid culture

Lineage depleted CB cells were stored in IMDM with 50% FCS and 10% DMSO at −150°C until use. CB cells were expanded *in vitro* in X-VIVO 10 (Bio Whittaker) supplemented with 1% BSA, 2 mM L-Glutamine, 100 U ml penicillin-streptomycin, and cytokines: SCF (50ng/ml), G-CSF (5ng/ml), FLT3L (50ng/ml), TPO (7.5ng/ml) and IL-6 (5ng/ml). TLS-ERG-immortalized CB (TEX) cells were expanded in IMDM with 15% FBS, 200mM L-glutamine, SCF (100ng/mL), IL-3 (10ng/mL) (Warner et al., 2005). The AML cell line 8227 was cultured in X-Vivo media supplemented with cytokines as described (Lechman et al., 2016).

Mouse xenotransplantation

Animal work was carried out in accordance with guidelines approved by the University Health Network Animal Care Committee. 8-11 week-old male NOD/Lt-scid/IL2Rγnull (NSG) mice were sublethally irradiated (225 cGy using a 137Cs γ-irradiator) 24h prior to intrafemoral transplantation. CB cells were transduced, expanded *in vitro* for up to 4 days and injected into the right femur with 30 μl PBS (Figures 3B and 3C) or sorted into TagBFP$^+$ (bulk), TagBFP$^+$GFP-low and TagBFP$^+$GFP-high populations and injected at 10,000 or 30,000 cells per mouse (Figures 3D and 3E). Mice were euthanized after 8-11 weeks and the femurs were flushed with PBS with 2% FCS. Cells were stained for surface markers and analyzed for TagBFP$^+$CD45$^+$ engraftment. Human engraftment was scored as positive if the mouse BM had > 1% CD45$^+$TagBFP$^+$ cells. Primary AML samples were transduced overnight and transplanted at 100,000 or 300,000 cells per mouse into the right femur with 30 μl PBS. After eight weeks, primary mice were sacrificed and their BM was analyzed by flow cytometry. To evaluate functional LSC content, pooled BM cells were sorted and transplanted into secondary recipient mice at multiple cell doses. After 11 weeks, BM cells were analyzed by flow cytometry.

METHOD DETAILS

Lentiviral vectors

The ATF4 reporter was used as previously reported (van Galen et al., 2014a). Briefly, the plasmids ATF4.5: 5′ATF4.GFP (Addgene 21852), ATF4.12: 5′ATF4.uORF1^{AUA}.GFP (Addgene 21859), and ATF4.14: 5′ATF4.uORF1&2^{AUA}.GFP (Addgene 21861) were used to construct the bidirectional lentiviral reporter vectors ATF4^{rep}, the negative control ATF4.12^{rep}, and the positive control ATF4.14^{rep}. These three vectors are identical apart from uORF start codon mutations. For the "TagBFP only" control, *luciferase* was cloned downstream of the SFFV promoter. We used the transgene ratio between GFP and TagBFP to account for differences in basal translation (TGR = GFP mean fluorescence intensity / TagBFP mean fluorescence intensity) as a measure of reporter activity. To generate eIF2α^{S52A}-OE, we mutated codon 52 from Serine to Alanine in *EIF2S1* plasmid (Harvard plasmid clone HsCD00044214). Using Q5 Site-Directed mutagenesis kit (NEB E0554S) with mutagenic primers TAGTGAATTAGCCAGAAGGCG and AGAAGAATCATGCCTT CAATG, the desired mutated eIF2α^{S52A} was amplified and cloned downstream of the bidirectional minhCMV-SFFV promoter using the Gateway compatible pLBC-OM-RFCA vector that also expresses mOrange.

shRNA knock-down constructs

shRNA sequences were predicted based on the Sherwood algorithm (Knott et al., 2014). shRNA oligo's were ordered as Ultramers from IDT and PCR amplified using AmpliTaq Gold 360 Polymerase (ThermoFisher) with shRNA amplification primers (Table S3). The PCR product was subsequently digested with BamH1 and Mlu1 and cloned into the pLBC2 vector downstream of mCherry.

Quantitative PCR

Total RNA from cells was purified and DNase treated using the RNeasy Micro Kit (QIAGEN). RNA integrity was measured on the Agilent Bioanalyzer (RNA nano kit, RNA integrity scores were > 9). cDNA was synthesized using SuperScript VILO cDNA Synthesis Kit (ThermoFisher). Quantitative PCR analysis was performed on the LightCycler 480 Instrument II (Roche). All signals were quantified using the ΔCt method and were normalized to the levels of GAPDH unless otherwise indicated. See Table S3 for primer sequences.

Amino acid depletion

AA depleted media were provided by Dr. Hiromitsu Nakauchi (Stanford University). CB cells were transduced with the ATF4 reporter. After 24hrs, cells were washed and plated in various AA depleted conditions supplemented with 1% BSA, 100 U/ml penicillin-streptomycin, and cytokines: SCF (50ng/ml), G-CSF (5ng/ml), Flt3L (50ng/ml), TPO (7.5ng/ml), IL-6 (5ng/ml), and IL3 (10ng/ml). After 48h exposure to AA deficient media, cells were analyzed by flow cytometry.

Thapsigargin, cycloheximide, valproic acid, temsirolimus, and bortezomib

Compounds were purchased as follows: thapsigargin, Sigma-Aldrich, catalog number T9033; cycloheximide, Sigma-Aldrich, catalog number C7698; valproic acid Sigma-Aldrich, PHR1061, bortezomib, Cell Signaling catalog number 2204; temsirolimus,

Sigma-Aldrich, catalog number PZ0020. All compounds were resuspended in DMSO and stored at −20°C until use. Final DMSO concentration was ≤ 1% in both control and treatments groups. Cell counts and viability analysis were carried out after 30h of drug treatment and thapsigargin was used at 0.2 μM.

Mass spectrometry

CB cells were thawed through dropwise addition of 50% FBS, 50% X-vivo 10 and 1% DNase, washed, and stained for 30 minutes on ice either 1) with CD34 APC-Cy7 and CD38 PE-Cy7 at a 1:100 dilution to sort HSC/MPP versus progenitor cells, or 2) with CD45RA BB515, CD90 PE, CD10 APC, CD7 V450 at 1:50, and CD34 APC-Cy7 and CD38 PE-Cy7 at 1:200 dilution to sort HSC, MPP, MLP and GMP (Table S1). Equal amounts of sorted cells (100,000 for low-resolution sorts, 50,000 for high-resolution sorts) were processed for mass spectrometry analysis as described (Lechman et al., 2016). Label-free quantitation was used to derive protein intensities and resulting data was analyzed using MaxQuant (Cox et al., 2014; Cox and Mann, 2008). Protein quantities are shown in heatmaps of $\log_2$ detection values. Values were centered by subtracting row means.

Fluorescence-Activated Cell Sorting (FACS) and intracellular flow cytometry

Immunophenotyping for human hematopoietic cell surface markers was carried out using the following antibodies: APC-conjugated anti-CD45 (1:100 2D1), PE-conjugated anti-CD33 (1:100 P67.6) V450-conjugated anti-CD7 (1:50 M-T701), PE-Cy7-conjugated anti-CD38 (1:100 HB7), APC-Cy7-conjugated anti-CD34, Biotin-conjugated anti-CD135 (1:50), PE-Cy5-conjugated anti-CD49f (1:100), PE-conjugated anti-CD19 (1:100 SJ25C1), Biotin-conjugated anti-CD45RA (1:50), PE-Cy5 conjugated anti-CD90 (1:100). CB cells were stained with antibodies for 30 min at 4°C. FACS sorting was performed using FACSAria sorters, and FlowJo software was used for data analysis.

For intracellular flow cytometry, CB cells were fixed with 80% methanol for 5 min, permeabilized with 0.1% PBS-Tween-20 for 30 min and incubated in PBS with 10% goat serum and 0.3M glycine. Cells were stained with primary antibody (total eIF2α: Santa Cruz sc-133132, Phospho-eIF2α: Abcam 32157) for 30 min at room temperature and washed three times with PBS buffer by centrifugation at 300 g for 5 min each time. Secondary antibody (Alexa Fluor 488, Thermo Fisher Scientific A11034) was added to the cells at 1:500 dilution for 30 min at room temperature, the cells were washed three times and resuspended in PBS buffer for analysis.

Apoptosis and cell proliferation assays

For the apoptosis assay, CB cells were washed with PBS and diluted in 1X Annexin V binding buffer to 1×10^6 in 0.5ml. Cells were stained in Annexin V-FITC at room temperature in the dark for 15 minutes. For the proliferation assay, CB cells were incubated at 37°C with 10μM of EdU for one hour. Cells were then fixed and permeabilized, and EdU incorporation into newly synthesized DNA was detected using Pacific Blue Click-iT Plus EdU azide (ThermoFisher Scientific # C10636).

Immunofluorescence

CB cells were sorted based on CD34, CD38, and CD45RA. Cells were cytospun and fixed with 4% formaldehyde. Cells were then blocked with 1X PBS with 5% normal serum and 0.3% Triton X-100 for 1h and stained with primary antibody for 1h (total eIF2α: Santa Cruz sc-133132, Phospho-eIF2α: Thermo Fisher Scientific 701268). Fluorochrome-conjugated secondary antibodies (Alexa Fluor-488 and Alexa Fluor-555) were applied for 1h. Coverslips were applied to slides with Prolong® Gold Antifade Reagent with DAPI. Images were obtained using an Olympus FluoView 1000 Laser Scanning Confocal Microscope and analyzed using Olympus Fluoview 1.1. Fluorochrome-specific signal intensity was quantified and normalized to cell areas selected from n = 8 images per stain.

Western blot

$CD34^+$ CB cells were treated with 0.2 μM thapsigargin for 30 hours. GFP-low and GFP-high fractions were sorted and 50,000 cells were lysed with RIPA buffer (Thermo Fisher Scientific 899000) containing protease and phosphatase inhibitors (Thermo Fisher Scientific 78446). Samples were centrifuged at 12,000 g for 5 min at 4°C and supernatants were used in western assay. Protein concentration was measured by BCA protein assay (Thermo Fisher Scientific 23225). Western size assay was performed with ProteinSimple Wes separation instrument. Samples were prepared and resolved on the 12-230 kDa capillary cartridge according to manufacturer's instructions. Antibodies (Cell Signaling anti-ATF4 #11815 and anti-GAPDH #2118) were titrated on a lysate from $CD34^+$ CB cells prior to the experiment to determine the optimal dilutions, which was 1:5 for ATF4 and 1:200 for GAPDH (capillary western uses very concentrated samples requiring higher antibody concentrations than regular western blot). Note that we used a monoclonal C-terminal antibody that does not overlap with the ATF4-GFP fusion gene in the $ATF4^{rep}$ vector (Cell Signaling #11815).

Transcriptional analysis

Expression levels of *ATF4* and ATF4 target genes were assessed in CB microarray datasets that were previously reported (Laurenti et al., 2013). To display ATF4 expression, the $\log_2$ values of three probes were corrected (by adding 1.87, −2.43 and 0.56) to equalize each HSC1 value to the mean HSC1 value across the three probes (Figure 1E). To determine expression of ATF4 targets in CB progenitors, we started from a list of target genes that was previously defined by ER stress induction in mouse embryo fibroblasts followed by ATF4 and CHOP ChIP-seq and RNA-seq (Han et al., 2013). Considering our specific interest in ATF4, we only assessed 254 ATF4-specific target genes (Overlap: ATF4 ONLY), and not CHOP (103) or common (218) targets. Gene symbol conversion using

BioMart identified 225 human homologs. Of these 225 genes, we found that 54 were differentially expressed in HSC/MPPs (HSC1, HSC2 and MPP) compared to myeloid progenitors (CMP, GMP, and MEP, $p < 0.01$ by Student's t test) in previously reported microarrays (Laurenti et al., 2013). These 54 genes are shown in a heatmap (log_2, and centered expression values) and used for GSEA (Figures 1F, 1G, and 4B).

QUANTIFICATION AND STATISTICAL ANALYSIS

Statistical details are provided in the figure legends. Unless otherwise noted, mean ± standard deviation values are given and *P value*s are calculated by two-tailed unpaired Student's t test using Microsoft Excel (version 16.17). To compare engraftment levels, we performed Mann–Whitney U-tests, as these data do not show a normal distribution, using Prism software (version 7.0a; GraphPad). To analyze *in vivo* limiting dilution analysis, we used ELDA software (Hu and Smyth, 2009) (http://bioinf.wehi.edu.au/software/elda). For heatmaps of mRNA and protein expression, expression values from microarrays or MaxQuant were log_2 transformed, centered, and visualized using the image function and a blue to white to red color gradient using R statistical software (RStudio Version 1.1.456). Stars are used to indicate significance in the figures: * $p < 0.05$, ** $p < 0.01$, *** $p < 0.001$, **** $p < 0.0001$.

DATA AND SOFTWARE AVAILABILITY

The accession number for previously reported microarrays of CB progenitors is GEO: GSE42414 (Laurenti et al., 2013). The accession number for previously reported RNA-seq of AML fraction is GEO: GSE76009 (Ng et al., 2016). Mass spectrometry analysis of hematopoietic progenitor cells is in preparation for publication (E.M.S., S. Xie, A. Mitchell, K.B. Kaufmann, Y. Ge, E. Lechman, T. Kislinger, B.T. Porse, J.E.D., unpublished data).